THE JOURNAL OF PHYSICAL CHEMISTRY C

Article

pubs.acs.org/JPCC

A Strategy of Enhancing the Photoactivity of g-C_3N_4 via Doping of Nonmetal Elements: A First-Principles Study

Xinguo Ma,[†,‡] Yanhui Lv,[†] Jing Xu,[†] Yanfang Liu,[†] Ruiqin Zhang,[‡] and Yongfa Zhu*[,†]

[†]Department of Chemistry, Tsinghua University, Beijing 100084, China

[‡]Department of Physics and Materials Science, City University of Hong Kong, Hong Kong, China

Supporting Information

ABSTRACT: An effective structural doping approach has been described to modify the photoelectrochemical properties of g-C_3N_4 by doping with nonmetal (sulfur or phosphorus) impurities. Here, the substitutional and interstitial doped models of g-C_3N_4 systems were constructed with different doped sites, and then their dopant formation energies and electronic properties were performed to study the stability and visible-light photoactivity using first-principles density functional theory, respectively. Our results have identified that an S atom preferentially substitutes for the edge N atom of g-C_3N_4; however, a P atom preferentially situates the interstitial sites of in-planar of g-C_3N_4. Furthermore, it is demonstrated that the doping with nonmetal impurities reduces the energy gap to enhance the visible-light absorption of g-C_3N_4. The increased dispersion of the contour distribution of the HOMO and LUMO brought by doping facilitates the enhancement of the carrier mobility, while the noncoplanar HOMO and LUMO favor the separation of photogenerated electron−hole pairs. Especially, P interstitial doping shows a prominent potential due to the appearance of a new channel for carrier migration. It should be pointed out that the proper doping form should be controlled, so that reasonable photoelectrochemical properties can be achieved.

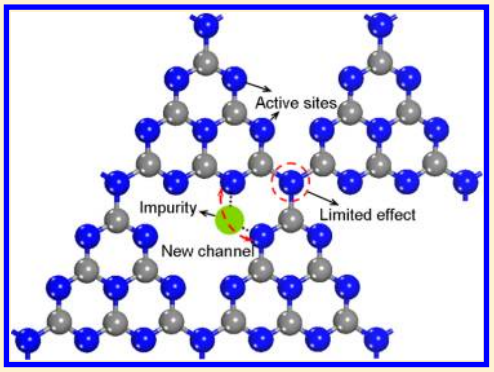

1. INTRODUCTION

An intense research activity has been devoted to search for active semiconductor photocatalysts that directly split water or degrade environmental pollutants under sunlight irradiation. Both strong light absorption and suitable redox potential are prerequisites for photocatalytic reaction.[1,2] Unfortunately, at present, most of semiconductors cannot meet all the criteria. TiO_2 has been dominantly used because of its high activation, long-term stability, low price, and availability, but its band gap is too wide to absorb sunlight efficiently. In the recent years, a growing interest was also focused on the non-TiO_2-based catalyzers, such as $InMO_4$ (M = Nb, Ta),[3] $BiVO_4$,[4,5] Bi_2WO_6,[6,7] $Ga_{1-x}Zn_xN_{1-x}O_x$,[8,9] Ag_2CrO_4,[10] $BiPO_4$,[11] and so on; however, the present achievements are still far from the idea goal. Recently, Wang et al. found a new use for graphitic carbon nitrides (g-C_3N_4) semiconductor, which can produce hydrogen from water under visible-light irradiation in the presence of a sacrificial donor.[12] The photodegradation performance of g-C_3N_4 obtained by heating low-cost melamine was investigated by Zou et al.[13] Their results indicate that for photodegrading dye the photocatalytic activities of g-C_3N_4 are higher than those of commercial nitrogen-doped TiO_2. Contrary to other conducting polymer semiconductors, g-C_3N_4 is chemically and thermally stable and does not rely on the complicated device manufacturing,[14−17] suggesting that the polymer semiconductor has huge potentials in photocatalysis fields.

Carbon nitride has been the subject of several experimental investigations.[16−23] Most of the work is devoted to the synthesis and characterization of its polymorphs. Carbon nitride can exist in several allotropes with diverse properties, but the graphitic phase is regarded as the most stable structure under ambient conditions. Kroke et al.[14,16] and Gracia et al.[24] indicated that planar graphitic model based on the hexagonal heptazine structural motif (C_6N_7) is lower in energy than structures based on the triazine (C_3N_3) motif. The structure stability and redox ability of g-C_3N_4 semiconductor stimulate us to explore its application as a new metal-free photocatalyst that directly splits water or degrades environmental pollutants under sunlight irradiation. However, low carrier mobility and insufficient sunlight absorption limit the energy conversion efficiency.[12] The another drawback of g-C_3N_4 is only moderate water oxidation ability due to its high level of the top of the valence band (VB) at about 1.4 eV vs NHE.[25]

Generally, chemical doping is an effective strategy to modify the electronic structures of semiconductors as well as their surface properties, thus improving their performances. A posteriori applied proton doping of g-C_3N_4 not only significantly changes its morphology and surface property but also tunes its electronic structure and enhances its ionic conductivity.[26] In addition, localization of electrons by the protons however leads to an increase of band gap value.[26] In fact, it is desirable that the band gap value of the semiconductor

Received: August 22, 2012
Revised: October 6, 2012
Published: October 19, 2012

would be about 2.0 eV to effectively utilize the visible light. A "structural doping" strategy has attracted people's attention. The geometry structure of g-C_3N_4 contains nitrogen triangles having six lone-pair electrons, which are available for nonmetal inclusion. Consequently, the doping of g-C_3N_4 with nonmetal impurities seems to be a feasible way to deal with these drawbacks mentioned above. Recently, an effective approach of sulfur-mediated synthesis was developed to modify the texture, optical and electronic properties, and photocatalytic functions of carbon nitride semiconductor.[27]

Principally, conjugated polymers with heteroatoms of higher periodic elements tend to have narrower band gaps and lower HOMO levels; e.g., polythiophene shows a reduced band gap and lower HOMO level than polypyrrole.[28] The big atomic size of sulfur (S) and phosphorus (P) is expected to influence the conformation and the connectivity of the resultant C_3N_4 polymer and hence offer a template tool to tune the texture and electronic structure.[27,29,30] Thus, we specifically constructed the doped systems with S or P impurity, including the substitutional and interstitial doped models, and calculated their dopant formation energies and electronic properties using first-principles density functional theory (DFT). The present study has three main objectives. First, by analyzing the electronic properties of pure g-C_3N_4, we try to reply why the material displays a relative poor performance of photocatalysis. Second, the validity of doped systems with S or P impurities is examined to obtain stable doped configuration. Finally, the effect of doping on electronic structures and optical properties of g-C_3N_4 is discussed in detail and correspondingly draws a proper doping strategy to overcome the difficulties of sunlight absorption and charge migration.

2. CALCULATION METHODS

First, the total energy calculations of four g-C_3N_4 systems with different connection patterns were performed using the projector augmented wave (PAW) pseudopotentials with the exchange and correlation in the Perdew–Burke–Ernzerhof (PBE)[31] formalism of DFT as implemented in the Vienna *ab initio* simulation package (VASP)[32] and using the plane-wave ultrasoft (PWUS) pseudopotentials with the exchange and correlation in Perdew–Wang (PW91) formalism[33] as implemented in the CASTEP code.[34] Then, geometry structure, the electronic structure, and optical properties of pure and doped g-C_3N_4 were performed using the PWUS pseudopotential method with the generalized gradient approximation (GGA).[33,34] In addition, the local density approximation (LDA-CAPZ) calculations were also taken to predict the equilibrium lattice parameters of g-C_3N_4.[35] In PAW calculations, a pragmatic method to describe correctly van der Waals interactions resulting from dynamical correlations between fluctuating charge distributions has been given by the DFT-D2 approach of Grimme.[36] In PWUS calculations, a hybrid semiempirical solution (OBS) was taken to introduce damped atom pairwise dispersion corrections of the form C_6R^{-6} in the DFT formalism.[37] The semiempirical approach provides the best compromise between the cost of first-principles evaluation of the dispersion terms and the need to improve nonbonding interactions in the standard DFT description. The valence atomic configurations are $2s^22p^2$ for C, $2s^22p^3$ for N, $3s^23p^4$ for S, and $3s^23p^3$ for P. A cutoff energy of 400 eV and a Monkhorst–Pack k-mesh of 8 × 5 × 8 are used. Geometry optimizations were done before single-point energy calculation, and the self-consistent convergence accuracy was set at 1×10^{-6} eV/atom. The convergence criterion for the maximal force on atoms is 0.02 eV/Å. The maximum displacement is 5×10^{-4} Å, and the stress is less than 0.02 GPa. The atomic Mulliken charge and bond overlap population were investigated using a projection of the plane-wave states onto a linear combination of atomic orbital (LCAO) basis set,[38] which is widely used to perform the population analysis of charge transferring.

3. RESULTS AND DISCUSSION

3.1. Pure g-C_3N_4. To determine the stable graphite-like C_3N_4 crystal, we constructed four graphitic carbon nitride networks with different connection patterns and then calculated their total energies, as shown in Figure 1. The calculated results

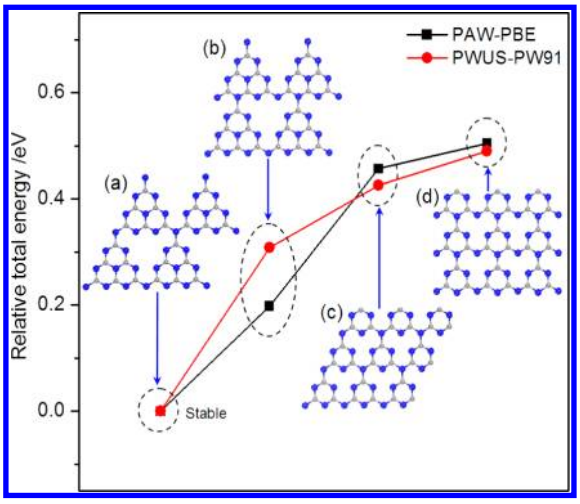

Figure 1. Relative total energy per C_3N_4 unit of pure bulk graphitic carbon nitride networks with different connection patterns. Heptazine-based structure: (a) hexagonal and (b) monoclinic, triazine-based structure; (c) hexagonal and (d) orthorhombic. The total energy per C_3N_4 unit of hexagonal heptazine-based g-C_3N_4 is the reference level to decide the relative stability of four different connection patterns. After geometry optimization, the monoclinic heptazine-based g-C_3N_4 shows a buckled structure. Gray and blue spheres represent the C and N atoms, respectively.

show that heptazine structural motif with hexagonal system is lowest in energy than other three structures. The experimental observation of highly ordered planar C_3N_4 precursors has verified our theoretical results.[12,15] Thus, in succedent work, we only investigated the pure hexagonal heptazine-based g-C_3N_4 and its doped systems. The most stable graphitic phase will crystallize in the hexagonal structure with space group *cmc*21 (No. 36), which is composed of nitrogen-linked heptazine units arranged in a graphite-like structure stacked in a staggered ABAB fashion, as shown in Figure 2. All C atoms experience 3-fold coordination by three N atoms. The bridge N atoms and inner N atoms are all 3-fold coordination by three C atoms; however, the edge N atoms are 2-fold coordination by two C atoms. By minimizing the crystal total energy, the equilibrium lattice parameters have been obtained using GGA and LDA methods incorporating the OBS correction, and the results are given in Table 1 with the other theoretical and experimental values. It is well-known that the latter approximation, LDA, underestimates the lattice constants and overestimates cohesive energies relative to the experimental values while the opposite is true for GGA. Gracia et al.[24] reported that the optimized g-h-Heptazine.aiMD structure shows in-planar distance of the

dx.doi.org/10.1021/jp308334x | J. Phys. Chem. C 2012, 116, 23485–23493

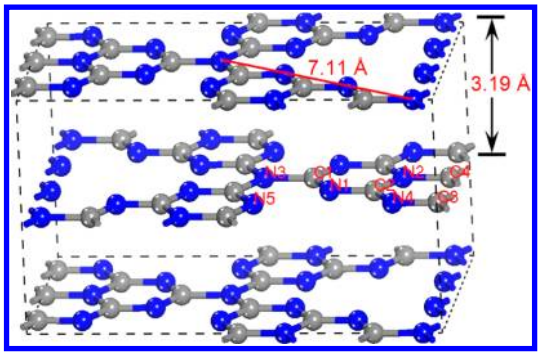

Figure 2. Unit-cell structure of hexagonal heptazine-based g-C_3N_4, including 56 atoms, 32 of which are N atoms and 24 are C atoms. Gray and blue spheres represent the C and N atoms, respectively. Roman numbers labeled on the C and N atoms are used to identify the special sites considered in this work.

nitride pores at the center of adjacent heptazine rings of 6.77 Å, which agrees with the in-plane repeat period of 6.81 Å from the XRD pattern reported by Wang et al.[12] However, both values are the same in contradiction to the results of Bojdys et al.,[15] where a = 7.30 Å at the same pattern. It is believed that the experimental lattice constants should be in the range of our two theoretical values using GGA and LDA methods. Thus, it can be conjectured that the in-planar distance of the nitride pores at the center of adjacent heptazine units and the interlayer distance of pure bulk g-C_3N_4 are about 7.11 and 3.19 Å, respectively. The former is in good agreement with the theoretical results of the g-C_3N_4 monolayer from refs 39 and 40. Our calculated results show that the interaction energy E_{inter} between two heptazine layers of g-C_3N_4 is 0.036 eV/Å^2, smaller than that of graphite (0.059 eV/Å^2) (see Figure S1 in Supporting Information). This indicates that the weak $\pi-\pi$ interaction is a van der Waals force between layers. Thus, there is easy chemical stripping to get a large surface area, which is an advantage of the photocatalytic reaction.

All optimized results calculated using GGA and LDA methods show that the bulk g-C_3N_4 has a stable planar configuration, which is different from the buckled geometry of the g-C_3N_4 monolayer.[39,41] Mostly the N−C bond length is about 1.33 Å, except for two: one is between 1.38 and 1.40 Å in the middle of heptazine unit, and one in which the nitrogen atom connects the three heptazine units is between 1.45 and 1.48 Å, as shown in Figure 3a. As for the chemical bonding behavior in g-C_3N_4, we simply performed the corresponding Mulliken charge and overlap population calculations to analyze the bonding character quantitatively (see Table 1 and Table S1). The transferred Mulliken charge from a C to round N atoms is about 0.50e, so each N atom obtains 0.37e (weighted average). Partial electron transferring is due to 0.5 of the electronegativity difference between C and N atoms on the Pauling scale.[42] The overlap populations for several nearest neighbors in the crystal shown in Table 1 are all positive values, indicating bonding states between C and N atoms, and a high value implies that there is significant covalent interaction with each other. It is obvious that the length of the edge bond is shorter than that of other bond, due to a low coordination of the edge N atoms and thus a higher covalent character. However, the N3−C1 bond shows a low covalent nature whose overlap population is 0.76e for GGA and 0.79e for LDA. So the bonds connecting the bridge N3 atom break more easily than other C−N bond of heptazine unit in the synthesis process.

Here, we need to mention that all electronic structures and optical properties of pure and doped g-C_3N_4 in succedent work were performed using the PWUS-PW91 method incorporating OBS correction. The energy band structure of pure g-C_3N_4 (see Figure S2) shows that the indirect band gap value of 1.19 eV is 1.51 eV smaller than the experimental value previously reported by Wang et al., due to the well-known limitation in DFT. We failed to correct the band gap of g-C_3N_4 system using the LDA +U approach because this approach is not proper to the covalent systems. In succedent work, a rigid scissors operation correction of 1.51 eV was taken to adjust the band gap of all g-C_3N_4 systems, including the doped systems with S or P atoms later.

Figure 4a shows total density of states (TDOS) and partially density of states (PDOS) spectra of pure bulk g-C_3N_4. It can be seen that the VB edge is mainly contributed by the triangular edge N atoms (e.g., N1 2p state) and also has some contribution from the inner N atoms (e.g., N2 2p state), while the conduction band (CB) edge consists mainly of 2p states of the inner N atoms and C atoms. In addition, the contribution of VB is minimal from the C atoms, which presents the little hybridization with the adjacent N atoms. Therefore, photogenerated e^-/h^+ pairs only appear at the N site. Additionally, C atom has a somewhat large contribution to the top of CB and is strongly hybridized with the N2 atom. To further clarity the complicated active sites of the system, we presented the orbital information associated with the selected states (i and ii, corresponding HOMO and LUMO orbitals, respectively) marked with ellipses in the TDOS of Figure 4a, as shown in Figure 4b,c. From the contour distribution, the HOMO is composed of 2p orbitals of low coordinated N atoms

Table 1. Structure Parameters and Bond Overlap Population of g-C_3N_4[a]

					bond length/Å			
method	a/Å	b/Å	c/Å	E_g/eV	N1−C1	N1−C2	N2−C2	N3−C1
PW91(GGA)	7.16	12.35	6.96	1.19	1.34 (1.04)	1.33 (1.04)	1.40 (0.81)	1.47 (0.76)
CAPZ(LDA)	7.06	12.25	5.78	0.71	1.33 (1.05)	1.32 (1.08)	1.38 (0.84)	1.45 (0.79)
expt[b]	6.91		6.52	2.70				
expt[c]	7.30		6.72					
other theory[d]	7.13	12.35	6.92					
other theory[e]	7.13		7.09					
other theory[f]	7.10			1.00	1.33	1.33	1.39	1.48

[a] E_g denotes band gap energy. The data in this work are gained using the PWUS method with PW91 and CAPZ formalism. The values in parentheses correspond to bond overlap population. [b] Wang et al. (ref 12). [c] Bojdys et al. (ref 15). [d] Gracia et al. (ref 24). [e] Pan et al. (ref 39). [f] Aspera et al. (ref 40).

dx.doi.org/10.1021/jp308334x | J. Phys. Chem. C 2012, 116, 23485−23493

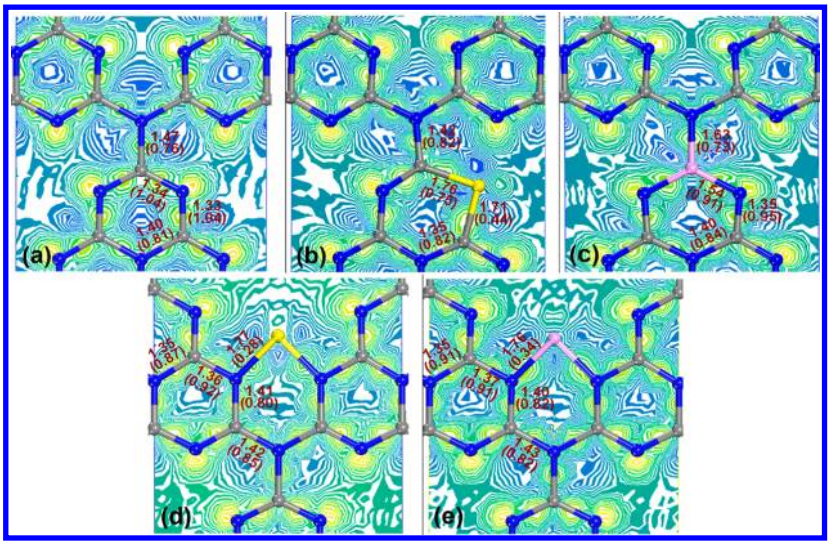

Figure 3. Difference charge density contour maps in planar and part of bond length and corresponding bond overlap population of g-C_3N_4 systems: (a) pure, (b) S_{N1}, (c) P_{C1}, (d) S_i, (e) P_i. Gray and blue spheres represent the C and N atoms, respectively. In addition, yellow and purple spheres represent the S and P atoms (impurities), respectively.

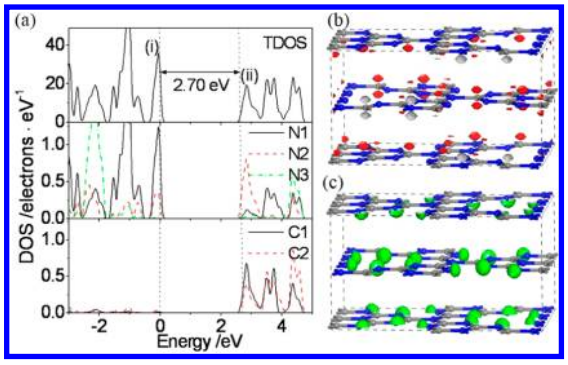

Figure 4. (a) TDOS and PDOS, (b) LUMO (upper red part), and (c) HOMO (lower green part) of pure g-C_3N_4. The Fermi level is set to the zero of energy. Gray and blue spheres represent the C and N atoms, respectively.

in planar, while the LUMO is mainly of C 2p character in the Z direction. Thus, the low coordinated N atoms would show oxidation activity in planar, while C atoms would show reduction activity in interlayer. However, the HOMO and LUMO show greatly localization on the low coordinated N atoms and round C atoms, respectively. Thus, the separation of photogenerated e^-/h^+ pairs is not very efficient.

Additionally, the N3 atom's contribution to either the VB or CB edge is insignificant, and its occupied states are mainly situated 0.6 eV below the Fermi level, while the major peak of the unoccupied N3 2p states is situated 1.35 eV above the CB edge, as shown in Figure 4a. Figure 4b,c clearly infers that there is no HOMO and LUMO on all bridge N atoms. Thus, any electrons and holes excited under near visible-light irradiation would not reach the bridge N atom. Here, the bridge N3 is a connecting atom among three heptazine units. These imply that the carriers transferring from one heptazine unit to another will be limited by the bridge N atoms. Unless the strength of sp^2-hybridization between bridge N and adjacent C is significant enough (thus delocalized) near the band edges, the intertriangular carrier migration would be suppressed greatly.[42] Consequently, the photogenerated electrons and holes in one heptazine unit would not take a catalytic reaction in any other area. It can be presumed that in terms of photocatalytic reactivity each heptazine unit behaves almost independently, which will reduce seriously the photocatalytic efficiency of g-C_3N_4. Therefore, it is desirable that a proper doping strategy can be designed to address these problems and thus improve photoelectrochemical properties of g-C_3N_4.

3.2. Formation Energies. In thermodynamic equilibrium, the concentration c of point defects is given by the expression $c = N_{site}N_{config} \exp(-E_f/kT)$.[43] Here, E_f is the defect formation energy, and lower E_f means to higher defect concentration c, which directly determines physical and chemical behavior of g-C_3N_4. In other words, defects with lower formation energies are more likely to form. To explore the possibility of doping and optimal growth conditions, the calculations of the dopant formation energies have been performed, according to the expression[43,44]

$$E_f = E_T^q(\text{doped}) - E_T^q(\text{undoped}) - n_{\text{impurity}}\mu_{\text{impurity}} + n_C\mu_C + n_N\mu_N + q(E_{VBM} + E_F) \quad (1)$$

where E_T(doped) and E_T(undoped) are the total energies of the doping systems containing the impurities and of the pure host supercell, respectively. μ_{impurity} is the chemical potentials of the impurity elements; μ_C (μ_N) is that of C (N). n_{impurity} is the number of substitutional or interstitial impurity atoms. The dopant formation energy depends on growth conditions, which may be varied from C- to N-rich. For g-C_3N_4, μ_C and μ_N satisfy the relationship $3\mu_C + 4\mu_N = \mu$(g-C_3N_4). Here, gas N_2, P_4, and S_8 molecular, solid graphite (4 atoms in a unit cell) are used to determine the chemical potentials: $\mu_N = \mu(N_2)/2$, $\mu_P = \mu(P_4)/4$, $\mu_S = \mu(S_8)/8$, $\mu_C = \mu$(graphite)/4. In order to study the relation between the dopant formation energies and the chemical potential of N element, the formation enthalpy ΔH_f[g-C_3N_4] is expressed as ΔH_f[g-C_3N_4] = $3\Delta\mu_C + 3\Delta\mu_N = 3(\mu_C - \mu_{C[\text{graphite}]}) + 4(\mu_N - \mu_{N[N_2]})$. In this work, ΔH_f[g-C_3N_4] = −0.49 eV; thus −0.12 eV ≤ $\Delta\mu_N$ ≤ 0. In other words, $\Delta\mu_N$ = 0 eV indicates under extreme N-rich condition; $\Delta\mu_N$ = −0.12 eV indicates under extreme C-rich condition. Here, the formation enthalpy of g-C_3N_4 is very low, which is greatly smaller than that of anatase TiO_2 (−10.3 eV) calculated using

dx.doi.org/10.1021/jp308334x | J. Phys. Chem. C 2012, 116, 23485−23493

the GGA method in ref 45. This indicates that the growth conditions have a little effect on the defect concentration. In succedent work, the effect of the growth conditions on the dopant formation energies was not considered.

To study the influence of various dopant concentrations on the defect formation energy of the g-C_3N_4 crystal, we calculated the defect formation energies of five interstitial models with different dopant concentrations from 0.89% to 7.14%, as shown in Figure 5. The results show that the formation energy per dopant atom is small and has a slow increasing function of the dopant concentrations. As a consequence, the synthesis of the nonmetal doped system with a high doped level becomes relatively easy in the experiment because low dopant formation energy is required. Figure 5 shows that the convergence of the formation energy per dopant atom is about 0.02 eV at dopant concentration of 1.79% for the S_{in}- or P_{in}-doped system. Thus, the size of 56-atom unit cell used is believed to be large enough to describe the essential features of the nonmetal doped systems. To determine the stable doped structures of g-C_3N_4, we constructed several doped configurations based on substitutional and interstitial doped models with S or P impurity and then calculated their total energies. Five N sites and four C sites are labeled with numbers N1—N5 and C1—C4, respectively, as shown in Figure 2. Table S1 lists fractional coordinates of these atoms. In fact, for monodoping, only three N sites (N1, N2, N3) and two C sites (C1, C2) need to be considered in several possible doped configurations with S or P atoms, including substitutional and interstitial doping case.

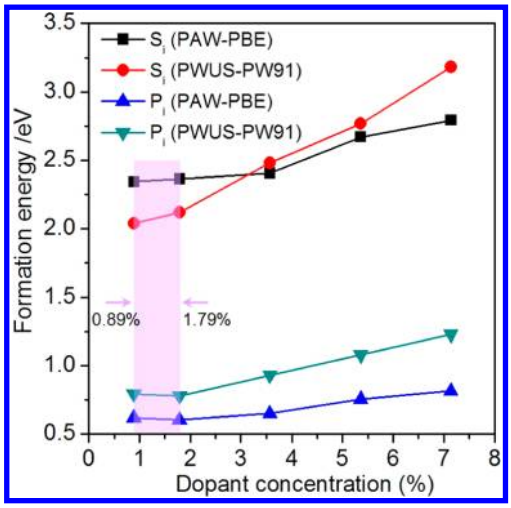

Figure 5. Lowest formation energy of S or P interstitial in g-C_3N_4 at each dopant concentration using the PAW-PBE and PWUS-PW91 formalisms of DFT, respectively. The dopant concentration in purple region would be reliable in this work.

The dopant formation energies of P- or S-doped g-C_3N_4 are shown in Table 2. Here, we considered two charge states (0, +1) to compare the stability of doped configurations. There are several features: (1) all the dopant formation energies of P- or S-doped g-C_3N_4 with +1 charge state are lower than those with 0 charge state, indicating that the doped configurations with +1 charge state are energetically stable (see Figure S3). (2) The dopant formation energies of S_{N1}-doped g-C_3N_4 are lower than those of S_{N2}- or S_{N3}-doped g-C_3N_4 (the differences are 4.9 and 2.3 eV for +1 charge state, 4.67 and 2.24 eV for 0 charge state, respectively), indicating that the S_{N1}-doped configuration is energetically favorable to other S substitutional doped configurations, which is in good agreement with the refs 27 and 29. It is interesting that the dopant formation energy of S interstitial (S_i) doped configuration is only 0.35 eV higher than that of S_{N1}-doped configuration. (3) For P-doped g-C_3N_4, the dopant formation energy of P_{C1}-doped configuration is more energetically favorable than all other substitutional cases. However, it is worth noting that the dopant formation energy of P interstitial (P_i)-doped configuration is almost equal to that of P_{C1}-doped configuration (the difference is 0.02 eV). Both of them are negative, which indicates that these doping will form spontaneously.

Previously partial experimental results present that the S atom preferentially substituted for the N1 atom;[27,29] however, the P atom preferentially substituted for the C1 atom.[30] The former is supported by our calculated results. The latter is in dispute. The structural details on the incorporation of P into the C/N scaffold were obtained with energy dispersive X-ray microanalysis and X-ray photoelectron spectroscopy measurements by Zhang et al.[30] From the measured data, we presumed that at least part of P atoms should adsorb in a large hollow space of planar structure. There are two points to be considered: (1) Elemental analysis shows that the C/N ratios of g-C_3N_4 before and after doping are quite similar to the theoretical value for g-C_3N_4 (0.75). By increasing the initial BmimPF6 portion, C/N is slightly increased. In fact, the data imply that the phosphorus heteratoms do not probably replace the corner carbon (C1) or bay carbon (C2) forming a P−N bond in the doped C_3N_4 framework, for the substitutions of phosphorus for lattice carbon should induce a decreasing of the C/N ratios of g-C_3N_4. (2) The P_{2p} binding energy peaks of P-doped g-C_3N_4 are centered at ca. 133.5 eV, which is typical for a P−N coordination. The vibrations of the P-related groups were hardly observed in doped g-C_3N_4 except for those of P−N stretching mode. Our analyzed results are not in complete agreement with the conclusion of substitutional doping from Zhang et al.[30] If some detailed experimental data of P−N bond length can be obtained, the conclusion will become clear. Because the P−N bond length in P_i-doped configuration is more than 1.70 Å, which is greatly larger than those in P_{C1}-doped configuration (about 1.58 Å). In succedent work, we only focused the lower energy configurations of P- or S- doped systems. In every case, the geometry optimization was always made, and the convergence is assured when the forces on atoms are less than 0.02 eV/Å, based upon which the electronic structures are calculated.

3.3. Band Edge Potentials. To give direct analysis, the band edge potentials of the CB and VB of g-C_3N_4 can be

Table 2. Dopant Formation Energies (eV) of g-C_3N_4 Using the PWUS-PW91 Method Incorporating OBS Correction[a]

charge state	S_{N1}	S_{N2}	S_{N3}	S_i	P_{C1}	P_{C2}	P_{N1}	P_{N2}	P_{N3}	P_i
0	1.76	6.43	4.00	2.12	0.73	1.52	1.33	3.55	1.93	0.78
+1	0.47	5.33	2.76	0.82	−0.55	0.40				−0.53

[a]Two charge states were considered in this work.

dx.doi.org/10.1021/jp308334x | J. Phys. Chem. C 2012, 116, 23485−23493

estimated from the absolute electronegativity of the atoms and the band gap of the semiconductor by eq 6 of ref 46 and eq 2 of ref 47. The results suggest that the CB and VB edge potentials of g-C_3N_4 are about −1.05 and 1.65 V vs NHE at pH = pH_{ZPC} (corresponding to that in aqueous solution, the net adsorbed charge of the sample obtained in an electrolyte is zero), respectively. The scale factor E_0 is 4.44 V relating the reference electrode redox level to the absolute vacuum scale (AVS).[46,47] In general, at T = 298 K and 1 atm, a great many of semiconductors (e.g., Ta_3N_5, GaN) react with H^+ or OH^- ions in solution, and the band edges at the interface consequently shift with the pH of the solution, about 60 mV per pH unit change,[46−48] which is due to surface ionization driven by adsorbed species (e.g., H^+ and OH^-). If the pH_{ZPC} of g-C_3N_4 can be obtained, we can estimate the CB and VB edge potentials of g-C_3N_4 for different pH value at ambient conditions. The valence band X-ray photoelectron spectroscopy spectrum of g-C_3N_4 indicates that the position of the VB edge locates at about 1.53 V,[49,50] which is smaller than 2.16 V measured by the recorded ultraviolet photoelectron spectra of g-C_3N_4.[29] However, these results are larger than 1.45 V vs NHE (1.25 V vs Ag/AgCl at pH 6.6) determined by electrochemical Mott−Schottky plots.[27] The VB edge is more positive than the redox potential of RhB (1.43 V).[51] This ascertains that for photodegrading RhB in the g-C_3N_4 system direct photogenerated hole oxidation is energetically possible. However, this also means that the photogenerated holes are not incapable of directly oxidizing adsorbed hydroxyl groups generating hydroxyl radicals (2.7 V vs NHE).[50] It is known that absolute electronegativities of both S and P are smaller than those of both N and C. According to the average electronegativity theory to estimate the CB edge potentials, the S- or P-doping should induce a downshifting of the CB edge. The change trend is in agreement with the experimental results of ref 27. Additionally, the band edge potentials can also be adjusted by morphology, including bulk or mesoporous g-C_3N_4, etc.[52]

3.4. Substitutional Configurations. The relaxed lattice parameters of doped g-C_3N_4 were calculated to find out the effect of doping on their geometry structures. Table S2 shows that the interlayer distance and in-planar distance of the nitride pores in S_{N1}-doped configuration are smaller than those in pure g-C_3N_4. For the former, the trend of the effect of S doping on geometry structure is not in complete agreement with the experimental results of ref 27. Previously experimental studies show that the effect of preparation process on the structure is prominent,[53] especially the temperature factor, possible due to a weak $\pi-\pi$ interaction between heptazine layers. Figure 3b presents that the S−C1 and S−C2 bond lengths are larger than the average N−C bond length, being related to a large ionic radius of sulfur and a large hollow space in planar. For S_{N1} doping, S atom bonds with two C atoms, leaving two lone-pair electrons around S atom. The covalent character of two single bonds S−C is obviously weaker than original N−C bond, so the carbon round exists no localized positive charges (see Figure S4). At this point, the P_{C1}-doped system shows a similar character with S_{N1}-doped system. For P_{C1}-doped configuration, there is also a significant effect of P_{C1} doping on geometry structure. The average P−N bond length is about 1.58 Å, which is +6.8% larger than the average C−N bond length; however, the heptazine unit has a slight distortion. Combining the overlap populations and DOS, after substitutional doping, there is the bond type variation between C and N atoms (see Figure S4).

To compare modification in the electronic structure of different doped systems, the TDOS and PDOS of S_{N1}- or P_{C1}-doped g-C_3N_4 were calculated. Figure 6a shows that one

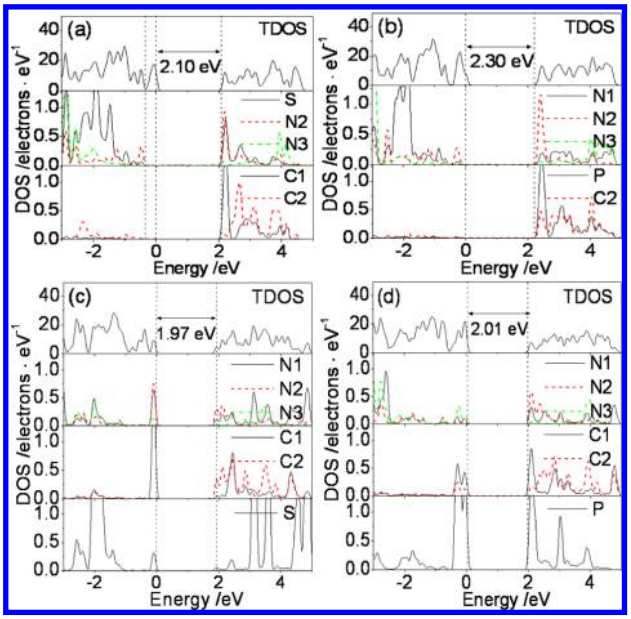

Figure 6. TDOS and PDOS of doped g-C_3N_4: (a) S_{N1}, (b) P_{C1}, (c) S_i, (d) P_i. The Fermi level is set to the zero of energy.

isolated S 3p state is localized just 0.18 eV below the bottom of the CB of the host g-C_3N_4 because S is much less electronegative than C, and the downshifting of CB edge is only 0.41 eV. There are no new S 3p states found at the top of VB while 2p states of C1 and C2 atoms in the VB have an obvious downshifting (about 0.3 eV). Thus, it can be predicted that the energy gap is about 2.1 eV. These results reveal typical n-type characteristics for the doped g-C_3N_4 semiconductor. Lowering the intrinsic VB to overcome the kinetic limitation against oxidation of water is another path to improve efficiency. It is reasonable to consider that S-derived localized energy state below the bottom of CB can be expected to significantly influence the optical absorption properties. In addition, under high impurity concentration, S_{N1} doping would create a partially occupied impurity band in band gap of the host g-C_3N_4 due to excess one electron on S 3p levels. It would be proved that the increase of S_N to S_N^+ occurs in S substitutional doped g-C_3N_4 due to the charge imbalance between S^{2-} ions and N^{3-} ions. Figure 7a shows that the delocalization of the HOMO and LUMO of S_{N1}-doped g-C_3N_4 becomes slightly stronger than that of pure g-C_3N_4.

The electronic structure of P_{C1}-doped g-C_3N_4 is similar to that of S_{N1}-doped g-C_3N_4. It is clear from Figure 6 that one isolated P 3p state are localized just 0.15 eV below the bottom of the CB of the host g-C_3N_4 because P is much electronegative than C, and the downshift of CB edge is no more than 0.25 eV, almost without altering the VB edge. Thus, the energy gap is about 2.3 eV. Although the maximum values of the energy gap reduction by S_{N1} and P_{C1} doping are about 0.6 and 0.4 eV, corresponding to the extension of the absorption edge about 130 and 80 nm, respectively. The p electrons of the N3 atom connecting three heptazine units are greatly localized to the atom, and its hybridization with neighboring C atoms is very weak. So any photogenerated electrons and holes under the near visible-light irradiation would not reach the N3 atom.

dx.doi.org/10.1021/jp308334x | J. Phys. Chem. C 2012, 116, 23485−23493

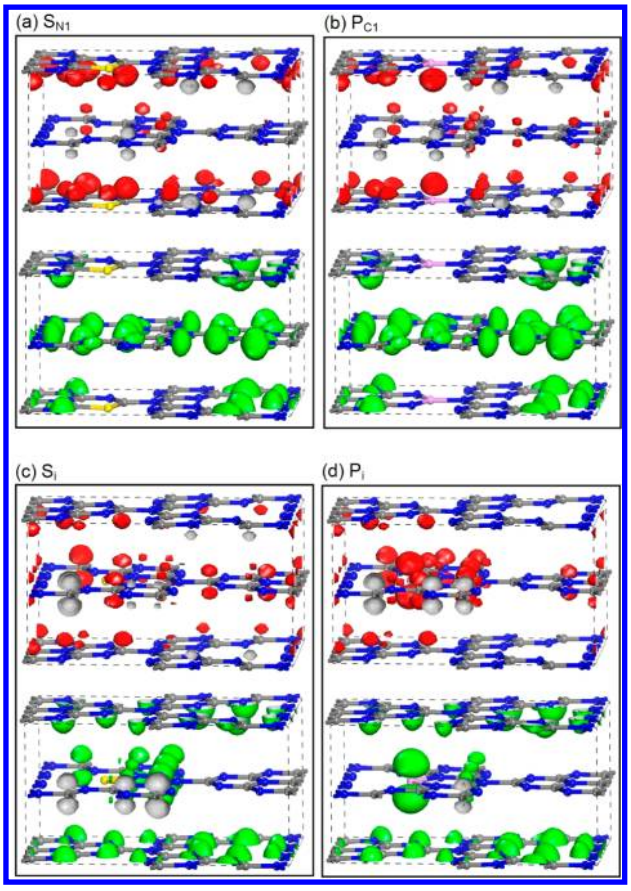

Figure 7. LUMO (upper red part) and HOMO (lower green part) of doped g-C_3N_4: (a) S_{N1}, (b) P_{C1}, (c) S_i, (d) P_i. The Fermi level is set to the zero of energy. Gray and blue spheres represent the C and N atoms, respectively. In addition, yellow and purple spheres represent the S and P atoms (impurities), respectively.

Thus, the separation of photogenerated e^-/h^+ pairs is not very efficient due to their short lifetime. Although the reaction rate is improved by substitutional doping, however, they are still only on a moderate level. To change the situation, the electronic structures of the interstitial doped configurations with S or P impurities were calculated to further analyze the effect of doping on the photocatalytic activity of g-C_3N_4.

3.5. Interstitial Configurations. In this work, the interstitial sites of in-planar and out-planar of g-C_3N_4 were examined in detail, and the dopant formation energies were calculated using eq 1. The results show that the S or P atom prefers to bind two edge N atoms in planar, as shown in Figure 3d,e. Table S2 shows that the interlayer distance and in-planar distance of the nitride pores for S_i- or P_i-doped g-C_3N_4 are also smaller than those for pure g-C_3N_4. Two S−N bond lengths are 1.77 Å for S_i-doped configuration, and two P−N bond lengths are 1.76 Å for P_i-doped configuration. The atomic Mulliken charge of S atom in interstitial doped configuration is 0.60*e*, which is almost equal to that of P atom in interstitial doped configuration. The interstitial atoms affect the original geometry structure little, especially S interstitial systems, due to a large hollow space in plane and a weak $\pi-\pi$ interaction between layers. For S_i doping, S bonds with two N, leaving two lone-pair electrons around S. Two S−N single bonds show obviously a weaker covalent character than other N−C bond; the absence of an electron around the carbon induces the positive charges around carbon. However, for P_i doping, two sp^2 hybrid orbitals of phosphorus bond with two sp^2 hybrid orbitals of adjacent nitrogen, while a lone-pair electrons localize round P atom and an electron delocalizes around N−P−N chain (see Figure S4). The results indicate that the shape of C−N═C chain is determined by a competition between the energy gain by extending the π-electron system into the chain and the repulsion between the lone-pair electrons on the edge N atom of the heptazine unit.[54,55]

More detailed information can be found from the TDOS and PDOS of S_i-doped systems. Figure 6c shows that the VB edge is partially contributed by 2p states of N1 and N2 atoms and also has some contribution from the C1 atom, which is different with the results of S_{N1}-doped configuration mentioned above, while the CB edge consists partially of 2p states of N1, N2, and C2 atoms. It is noted that the contribution of VB and CB edge is minimal from the S and N3 atoms, which have a little hybridization with the adjacent C atoms, as shown in Figure 7c. The calculated energy gap value is about 1.97 eV. Comparing with the pure g-C_3N_4, the S_i doping induces more activity sites. So, it can be argued that electrons would be most likely excited under visible-light irradiation from the N and C atoms and would reach the hybridized N/C 2p state at the CB edge. However, the photogenerated carriers under visible-light irradiation cannot move freely between two neighboring heptazine units because the S and bridge N3 atom's contribution to either the VB edge or CB edge is almost nothing.

The P_i-doped configuration shows a relatively low dopant formation energy, and thus the appearance of interstitial doping is energetically favorable. The PDOS of P_i-doped configuration is a little different with that of S_i-doped configuration, as shown in Figure 6d. The contribution of 2p states of N1 and N2 atoms to the VB edge decrease a lot, however, and there is an increased contribution of 2p states of N1 and N2 atoms to the CB edge. The p states of P and C1 atoms contribute both the VB and CB edges of P_i-doped g-C_3N_4, and thus electrons in the VB edge can be excited from the P and C1 atoms. Accordingly, the energy gap value of the P_i-doped configuration is similar to that of the S_i-doped configuration because these doping systems have same framework structure mentioned above. Figure 7d clearly infers that the HOMO and LUMO are greatly delocalized around P and adjacent N atoms. Thus, there is reason to believe that photogenerated carriers under visible-light irradiation transfer freely by the way of C−N−P−N−C chain between two adjacent heptazine units. This will greatly prolong the lifetime of photogenerated carriers and thus decrease the limited effect of the bridge N atoms on the carrier mobility. The increased dispersion of the contour distribution of the HOMO and LUMO brought by doping will enhance the carrier mobility. In addition, the noncoplanar HOMO and LUMO favor the separation of photogenerated e^-/h^+ pairs.[56] It is evident from the fact that no contribution of s orbitals is near the band edges, so the band edges are mainly made of 2p orbitals of C and N atoms.

3.6. Optical Absorption. The study of the optical properties of g-C_3N_4 is very necessary in visible-light photocatalytic realm. The absorption coefficient indicates the fraction of energy lost by the electromagnetic wave when it passes through a unit thickness of the material, and it is proportional to the rate of Joule heat produced in the sample. We obtained the spectra by calculating the imaginary part of the complex dielectric function using eq 1 of ref 57 using the GGA method. The allowed transitions are determined by the nonzero matrix

dx.doi.org/10.1021/jp308334x | J. Phys. Chem. C 2012, 116, 23485−23493

elements of position operator. Here, the optical calculations were performed using plane polarization with the specified polarization direction where the E field vector parallel to axes a, b, and c (marked as $E\|a$, $E\|b$, and $E\|c$) and the "polycrystalline" polarization where the E field vector is an isotropic average over all directions. In the calculations of the spectra a small smearing of 0.1 eV was used to better distinguish the absorption peaks.

Figure 8 shows the total and polarized optical absorption spectra for the pure and doped g-C_3N_4. For the pure g-C_3N_4, it

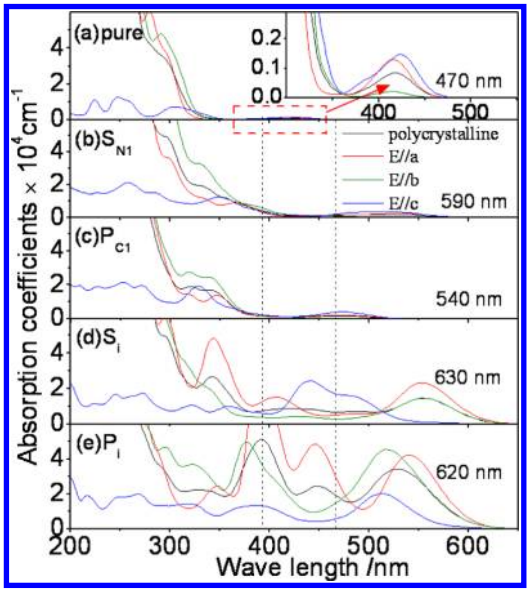

Figure 8. Calculated total and polarized optical absorption coefficient spectra of g-C_3N_4: (a) pure, (b) S_{N1}, (c) P_{C1}, (d) Si, (e) P_i. The inset shows an enlarged absorption coefficient spectra of pure g-C_3N_4 in the range from 300 to 550 nm.

is noted that a small peak between 370 and 470 nm is mainly contributed by the absorption spectra under $E\|a$ and $E\|c$. The absorption spectrum under $E\|b$ shows a weaker peak than those under $E\|a$ and $E\|c$ in the visible-light region, which attributes to a delocalized electron transition, not relevant to crystal structure. However, in the short wave region, the absorption spectrum under $E\|c$ is obviously different from those under $E\|a$ and $E\|b$. This is surely reasonable since the symmetry of the absorption spectra correspond to the symmetry of the lattice structure.[58] The inset of Figure 8 clearly show that the absorption edge of pure g-C_3N_4 corresponding to the largest wavelength is about 470 nm. This denotes that g-C_3N_4 is a visible-light semiconductor photocatalyst. However, the absorption intensity of pure g-C_3N_4 is so weak in the visible-light region that the visible-light absorption is not enough to contribute to the highly photocatalytic activity of g-C_3N_4.

It can be seen from the curve of the optical absorption spectra of substitutional doping systems that the absorption edges extent to 590 nm for S_{N1} doping and 540 nm for P_{C1} doping, respectively. Compared with the pure g-C_3N_4, the absorption intensity of substitutional doping systems increases a little in the visible-light region due to large dispersion of CB and some shallow donor levels in the band gap induced by S_{N1} and P_{C1} impurities, and thus their visible-light absorption still is not enough to contribute to the highly photocatalytic activity of g-C_3N_4. Zhang et al. found that for the CNS sample an obvious dopant-like absorption extending to about 580 nm was observed, due to the optical transition of the S impurity within the band gap,[27] which is in good agreement with that of our S_{N1}-doped system.

Figures 8d and 8e show the optical absorption spectra of S_i- and P_i-doped g-C_3N_4, respectively. It is interesting that both S_i and P_i monodoping induce an increase of optical absorption range (the absorption edges about 630 nm for S_i doping and 620 nm for P_i doping, corresponding to a photo transition energy of about 1.97 and 2.01 eV from the top of VB to the impurity levels below the CB),[30] and the absorption intensity of S_i- or P_i-doped g-C_3N_4 in the visible-light region greatly exceeds that of the pure g-C_3N_4 and substitutional doped systems. Therefore, the shallow impurity levels in the band gap of g-C_3N_4 will play a significant role in the increase of visible-light absorption. The red shift of the absorption edges of S_i- or P_i-doped g-C_3N_4 indicates that interstitial doping is different from protonation in which the spectrum is blue-shifted,[26,59] which supports our view that S or P is not bound as a counterion S or P ion, but indeed doped into the C−N matrix. Compared with the pure g-C_3N_4, it is noteworthy that S_i or P_i doping induces an increase of absorption spectra under $E\|a$ and $E\|b$ in the visible-light region. However, the absorption spectra under $E\|c$ are complex due to some delocalized electrons excited from the hybridized sp^2 orbitals. In addition, all calculated results imply that the absorption spectra of g-C_3N_4 systems have certain anisotropy in the short wave region.

4. CONCLUSIONS

We have proposed the use of doping with nonmetal impurities to improve photocatalytic property limitation of g-C_3N_4. Aside from substitutional doped configurations, interstitial doped configurations are energetically favorable. The results show that the doping with nonmetal impurities facilitates the increase of visible-light absorption of g-C_3N_4, which is especially prominent for interstitial doped configurations due to the significantly altering of the connectivity pattern and topology of the g-C_3N_4 sheets. The increased dispersion of the contour distribution of the HOMO and LUMO brought by doping is expected to modify the carrier mobility, while the noncoplanar HOMO and LUMO favor the separation of photogenerated e^-/h^+ pairs and thus promote heterogeneous photocatalysis. Especially, P_i doping shows a prominent potential due to the appearance of a new channel for carrier migration. This study serves as an initial and important step toward more in-depth analysis of the photocatalytic activity of g-C_3N_4 material.

■ ASSOCIATED CONTENT

Supporting Information

Atom positions and atomic Mulliken charge of g-C_3N_4; lattice parameters of doped g-C_3N_4 with +1 charge states; the interaction energy and the distance between layers; the energy band structure of pure g-C_3N_4; the dopant formation energies of g-C_3N_4 as a function of the Fermi level; the description of the bond type variation and the net charge distribution. This material is available free of charge via the Internet at http://pubs.acs.org.

■ AUTHOR INFORMATION

Corresponding Author

*E-mail: zhuyf@mail.tsinghua.edu.cn; Tel: (+86)10-6278-3586; Fax: (+86)10-6278-7601.

Notes

The authors declare no competing financial interest.

■ ACKNOWLEDGMENTS

This work was supported by the National Natural Science Foundation of China (20925725, 50972070, and 51102150) and the National Postdoctoral Science Foundation of China (20100480254 and 201104085). The authors gratefully acknowledge Professor M. A. Van Hove for valuable discussions on this topic.

■ REFERENCES

(1) Chen, X. B.; Shen, S. H.; Guo, L. J.; Mao, S. S. *Chem. Rev.* **2010**, *110*, 6503−6570.
(2) Kudo, A.; Miseki, Y. *Chem. Soc. Rev.* **2009**, *38*, 253−278.
(3) Zou, Z. G.; Ye, J. H.; Sayama, K.; Arakawa, H. *Nature* **2001**, *414*, 625−627.
(4) Kudo, A.; Ueda, K.; Kato, H.; Mikami, I. *Catal. Lett.* **1998**, *53*, 229−230.
(5) Kohtani, S.; Tomohiro, M.; Tokumura, K.; Nakagaki, R. *Appl. Catal., B* **2005**, *58*, 265−272.
(6) Fu, H. B.; Zhang, S. C.; Xu, T. G.; Zhu, Y. F.; Chen, J. M. *Environ. Sci. Technol.* **2008**, *42*, 2085−2091.
(7) Shang, M.; Wang, W. Z.; Zhang, L.; Xu, H. L. *Mater. Chem. Phys.* **2010**, *120*, 155−159.
(8) Wei, W.; Dai, Y.; Yang, K. S.; Guo, M.; Huang, B. B. *J. Phys. Chem. C* **2008**, *112*, 15915−15919.
(9) Maeda, K.; Domen, K. *Chem. Mater.* **2010**, *22*, 612−623.
(10) Ouyang, S. X.; Li, Z. S.; Ouyang, Z.; Yu, T.; Ye, J. H.; Zou, Z. G. *J. Phys. Chem. C* **2008**, *112*, 3134−3141.
(11) Pan, C. S.; Zhu, Y. F. *Environ. Sci. Technol.* **2010**, *44*, 5570−5574.
(12) Wang, X. C.; Maeda, K.; Thomas, A.; Takanabe, K.; Xin, G.; Domen, K.; Antonietti, M. *Nat. Mater.* **2009**, *8*, 76−82.
(13) Yan, S. C.; Li, Z. S.; Zou, Z. G. *Langmuir* **2009**, *25*, 10397−10401.
(14) Kroke, E.; Schwarz, M.; Horath-Bordon, E.; Kroll, P.; Noll, B.; Norman, A. D. *New J. Chem.* **2002**, *26*, 508−512.
(15) Bojdys, M. J.; Müller, J.; Antonietti, M.; Thomas, A. *Chem.—Eur. J.* **2008**, *14*, 8177−8182.
(16) Kroke, E.; Schwarz, M. *Coord. Chem. Rev.* **2004**, *248*, 493−532.
(17) Fang, L. M.; Ohfuji, H.; Shinmei, T.; Irifune, T. *Diamond Relat. Mater.* **2011**, *20*, 819−825.
(18) Zou, X. X.; Li, G. D.; Wang, Y. N.; Zhao, J.; Yan, C.; Guo, M. Y.; Li, L.; Chen, J. S. *Chem. Commun.* **2011**, *47*, 1066−1068.
(19) Mitoraj, D.; Kisch, H. *Chem.—Eur. J.* **2010**, *16*, 261−269.
(20) Sakata, Y.; Yoshimoto, K.; Kawaguchi, K.; Imamura, H.; Higashimoto, S. *Catal. Today* **2011**, *161*, 41−45.
(21) Yan, H. J.; Huang, Y. *Chem. Commun.* **2011**, *47*, 4168−4170.
(22) Thomas, A.; Fischer, A.; Goettmann, F.; Antonietti, M.; Müller, J. O.; Schlögl, R.; Carlsson, J. M. *J. Mater. Chem.* **2008**, *18*, 4893−4908.
(23) Guo, Y.; Chu, S.; Yan, S. C.; Wang, Y.; Zou, Z. G. *Chem. Commun.* **2010**, *46*, 7325−7327.
(24) Gracia, J.; Kroll, P. *J. Mater. Chem.* **2009**, *19*, 3013−3019.
(25) Zhang, J. S.; Chen, X. F.; Takanabe, K.; Maeda, K.; Domen, K.; Epping, J. D.; Fu, X. Z.; Antonietti, M.; Wang, X. C. *Angew. Chem., Int. Ed.* **2010**, *49*, 441−444.
(26) Zhang, Y. J.; Thomas, A.; Antonietti, M.; Wang, X. C. *J. Am. Chem. Soc.* **2009**, *131*, 50−51.
(27) Zhang, J. S.; Sun, J. H.; Maeda, K.; Domen, K.; Liu, P.; Antonietti, M.; Fu, X. Z.; Wang, X. C. *Energy Environ. Sci.* **2011**, *4*, 675−678.
(28) Ma, J.; Li, S.; Jiang, Y. *Macromolecules* **2002**, *35*, 1109−1115.
(29) Liu, G.; Niu, P.; Sun, C. H.; Smith, S. C.; Chen, Z. G.; Lu, G. Q.; Cheng, H. M. *J. Am. Chem. Soc.* **2010**, *132*, 11642−11648.
(30) Zhang, Y. J.; Mori, T.; Ye, J. H.; Antonietti, M. *J. Am. Chem. Soc.* **2010**, *132*, 6294−6295.
(31) Perdew, J. P.; Burke, K.; Ernzerhof, M. *Phys. Rev. Lett.* **1996**, *77*, 3865−3868.
(32) Kresse, G.; Hafner, J. *J. Phys.: Condens. Matter* **1994**, *6*, 8245−8257.
(33) Perdew, J. P.; Wang, Y. *Phys. Rev. B* **1992**, *45*, 13244−13249.
(34) Segall, M. D.; Lindan, P. L. D.; Probert, M. J.; Pickard, C. J.; Hasnip, P. J.; Clark, S. J.; Payne, M. C. *J. Phys.: Condens. Matter* **2002**, *14*, 2717−2744.
(35) Ceperley, D. M.; Alder, B. J. *Phys. Rev. Lett.* **1980**, *45*, 566−569.
(36) Grimme, S. *J. Comput. Chem.* **2006**, *27*, 1787−1799.
(37) Ortmann, F.; Bechstedt, F.; Schmidt, W. G. *Phys. Rev. B* **2006**, *73*, 205101−205110.
(38) Segall, M. D.; Shah, R.; Pickard, C. J.; Payne, M. C. *Phys. Rev. B* **1996**, *54*, 16317−16320.
(39) Pan, H.; Zhang, Y. W.; Shenoy, V. B.; Gao, H. J. *Catalysis* **2011**, *1*, 99−104.
(40) Aspera, S. M.; David, M.; Kasai, H. *Jpn. J. Appl. Phys.* **2010**, *49*, 115703−115712.
(41) Deifallah, M.; MeMillan, P. F.; Cora, F. *J. Phys. Chem. C* **2008**, *112*, 5447−5453.
(42) Huda, M. N.; Turner, J. A. *J. Appl. Phys.* **2010**, *107*, 123703−123707.
(43) Van de Walle, C. G.; Neugebauer, J. *J. Appl. Phys.* **2004**, *95*, 3851−3879.
(44) Ma, X. G.; Lu, B.; Li, D.; Shi, R.; Pan, C. S.; Zhu, Y. F. *J. Phys. Chem. C* **2011**, *115*, 4680−4687.
(45) Ma, X. G.; Jiang, J. J.; Liang, P. *Acta Phys. Sin.* **2008**, *57*, 3120−3125.
(46) Xu, Y.; Schoonen, M. A. A. *Am. Mineral.* **2000**, *85*, 543−556.
(47) Chun, W. J.; Ishikawa, A.; Fujisawa, H.; Takata, T.; Kondo, J. N.; Hara, M.; Kawai, M.; Matsumoto, Y.; Domen, K. *J. Phys. Chem. B* **2003**, *107*, 1798−1803.
(48) Huygens, I. M.; Strubbe, K.; Gomes, W. P. *J. Electrochem. Soc.* **2000**, *147*, 1797−1802.
(49) Yan, S. C.; Lv, S. B.; Li, Z. S.; Zou, Z. G. *Dalton Trans.* **2010**, *39*, 1488−1491.
(50) Yan, S. C.; Li, Z. S.; Zou, Z. G. *Langmuir* **2010**, *26*, 3894−3901.
(51) Shen, T.; Zhao, Z. G.; Yu, Q.; Xu, H. J. *J. Photochem. Photobiol. A: Chem.* **1989**, *47*, 203−212.
(52) Zhang, Y. J.; Antonietti, M. *Chem.—Asian J.* **2010**, *5*, 1307−1311.
(53) Goettmann, F.; Fischer, A.; Antonietti, M.; Thomas, A. *Angew. Chem., Int. Ed.* **2006**, *45*, 4467−4471.
(54) Lotsch, B. V.; Döblinger, M.; Sehnert, J.; Seyfarth, L.; Senker, J.; Oeckler, O.; Schnick, W. *Chem.−Eur. J.* **2007**, *13*, 4969−4980.
(55) Sehnert, J.; Baervinkel, K.; Senker, J. *J. Phys. Chem. B* **2007**, *111*, 10671−10680.
(56) Fukuzumi, S.; Kotani, H.; Ohkubo, K.; Ogo, S.; Tkachenko, N. V.; Lemmetyinen, H. *J. Am. Chem. Soc.* **2004**, *126*, 1600−1601.
(57) Sheetz, R. M.; Ponomareva, I.; Richter, E.; Andriotis, A. N.; Menon, M. *Phys. Rev. B* **2009**, *80*, 195314−195317.
(58) Liu, T. Y.; Zhang, Q. R.; Zhuang, S. L. *Phys. Lett. A* **2004**, *333*, 473−477.
(59) Wang, Y.; Di, Y.; Antonietti, M.; Li, H. R.; Chen, X. F.; Wang, X. C. *Chem. Mater.* **2010**, *22*, 5119−5121.